CHAPTER 1

Solar radiation and light materials interaction

Vishal Singh[a], Ina Rayal[b], Priyanaka[b], Himani Sharma[b], Charu Dwivedi[c], Bharti Singh[a]

[a]Department of Applied Physics, Delhi Technological University, Delhi, India
[b]Department of Physics, School of Physical Sciences, Doon University Dehradun, Dehradun, Uttarakhand, India
[c]Department of Chemistry, School of Physical Sciences, Doon University Dehradun, Dehradun, Uttarakhand, India

1 Introduction

The supply and demand of energy determine the course of global development in every sphere of human activity. Sufficient supplies of clean energy are intimately linked with global stability, economic prosperity, and quality of life. Finding energy sources to satisfy the world's growing demand is one of society's foremost challenges for the next half-century. It is generally understood that current patterns of energy supply are nonsustainable, and that renewable energy, including solar energy, is bound to play a major role.

1.1 Solar radiation and its characteristics

Solar radiation, often called the solar resource, is a general term for the electromagnetic radiation emitted by the sun *(1,2)*. Solar radiation can be captured and turned into useful forms of energy, such as heat and electricity, using a variety of technologies and materials. The different parts of the electromagnetic spectrum as shown in Fig. 1.1 have very different effects upon interaction with matter and therefore serve different purposes *(3)*. Starting with low frequency radio waves, the matter is quite transparent. (As we can listen to our portable radio inside our home since the waves pass freely through the walls of the house and even through the person beside us.) As we move upward through microwaves and infrared (IR) to visible light (VIS) more, absorption increases. In the lower ultraviolet (UV) range, all the UV from the sun is absorbed in a thin outer layer of our skin. As we move further up into the x-ray region of the spectrum, we become transparent again, because most of the mechanisms for absorption are gone, we then absorb only a small fraction of the radiation, but that absorption involves the more violent ionization events. Each portion of the electromagnetic

Energy Saving Coating Materials
http://dx.doi.org/10.1016/B978-0-12-822103-7.00001-7

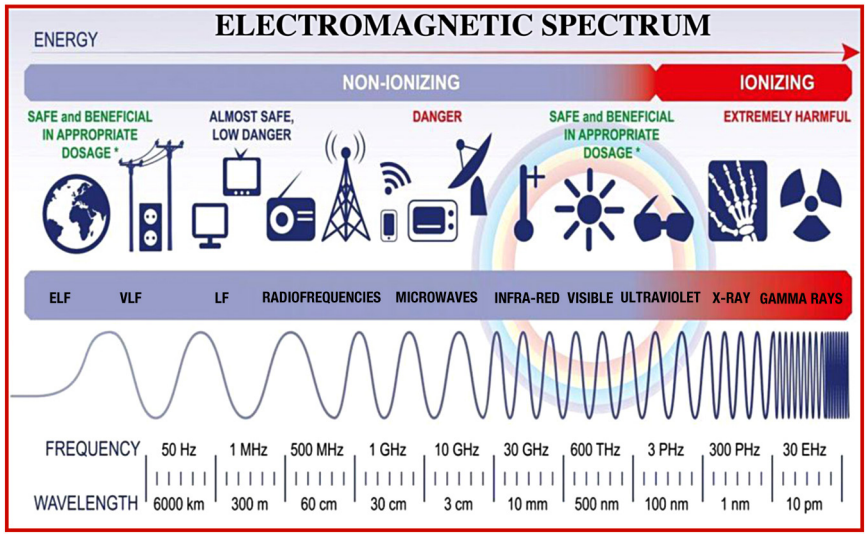

Figure 1.1 ***A diagram showing the electromagnetic spectrum.*** Source: (3) *Copyright.*

spectrum has quantum energies appropriate for the excitation of certain types of physical processes. The energy levels for all physical processes at the atomic and molecular levels are quantized, and if there are no available quantized energy levels with spacings, which match the quantum energy of the incident radiation, then the material will be transparent to that radiation, and it will pass through. If electromagnetic energy is absorbed, but cannot eject electrons from the atoms of the material, then it is classified as nonionizing radiation, and will typically just heat the material.

The spectrum of the incoming solar electromagnetic radiation (250-2500 nm) just outside the earth's atmosphere has a bell shape and defines the sun's temperature (~6000 °C) and is shown in Fig. 1.2 *(4)*. The total amount of energy emitted by the sun and received at the extremity of the Earth's atmosphere is constant-1370 $W/m^2/sec$. That received per unit area of the Earth's surface is 343 $W/m^2/sec$. Incoming solar radiations are absorbed by atmospheric gases such as O_2, O_3, CO_2, and H_2O vapor. UV light at wavelengths of <0.18 μm is strongly absorbed by O_2 at altitudes above 100 km (62 mi). Ozone below 60 km (37.2 mi) absorbs most UV between 0.2 and 0.3 μm (200-300 nm). Atmospheric absorption above 40 km (24.8 mi) results in attenuation of ~5% of incoming solar radiation. Under clear-sky conditions, another 10%-15% is absorbed by the lower atmosphere or is scattered back to space, with 80%-85% reaching the ground. It is important to note that the spectrum is limited to $0.25 < \lambda < 3$ μm so that there is no overlap with the spectrum of thermal radiation *(5)*. Hence, it is possible to

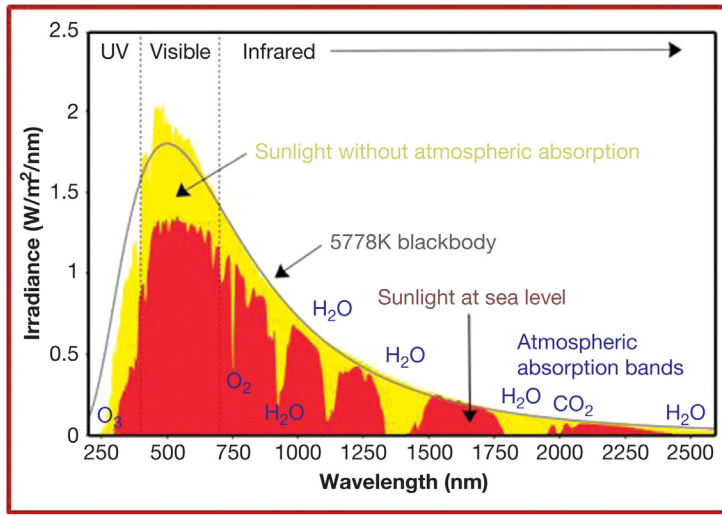

Figure 1.2 ***A diagram showing the solar radiation spectrum.*** Source: (5) *Copyright.*

have surfaces with properties being entirely different with regard to thermal and solar radiation. The balance between the incoming solar radiation and the outgoing thermal radiation is the base for our environmental conditions.

The incoming solar electromagnetic radiation carries energy in tiny packets, which are characterized by their frequency and are called photons. The famous Planck-Einstein relationship between photon frequency (ν) and the energy of E.M waves is given by equation

$$E = h\nu,$$

where h is a fundamental constant and is called as Planck's constant *(6)*. The value of "*h;*" = 6.626×10^{-34} Js. The wavelength and frequency dependence of photon energy is key in determining how it would interact with matter. Light traveling through a transparent media would travel at speed less than that of light in vacuum, that is, retardation is observed. An example cited earlier where a photon starting at the center of the sun took millions of years to reach the surface is due to this same interaction of photons with matter. Along its path, the photon undergoes a million collisions with the atoms, ions, of the matter, each time gaining or losing energy. But once it reaches the surface, it travels in the vacuum of space taking just 8.3 min to reach the Earth. All these different portions of E.M radiations interact very efficiently with matter. For example,VIS (and near-infrared light) is typically absorbed and emitted by electrons in molecules and atoms that move from one energy level to another. This action allows the chemical mechanisms

that underlie human vision and plant photosynthesis. If radiation having a frequency in the visible region of the EM spectrum reflects off an object, and then strikes the eyes, this results in visual perception of the scene. The brain's visual system processes the multitude of reflected frequencies into different shades and hues. This fine-tuned mechanism, a marvel of nature, is what allows us to "see." These types of interaction seem to be also dependent on the type of matter and change with bulk, thin films and nanomaterials. Hence, it becomes important to understand this solar radiation and matter interaction to get the benefit of a natural source of energy.

1.2 Importance of solar radiation

The world's major energy sources are nonrenewable and are faced with ever-increasing demand, and thus are not expected to last long. Besides being nonrenewable, these sources include mainly fossil fuels, contributing tremendously to the perennial problem of global warming because of CO_2 emission. The eminent depletion and pollution problems of the above energy sources make the international community focus attention on alternative sources of energy, especially solar energy appears highly promising. The sun is Earth's natural power source, driving the circulation of global wind and ocean currents, the cycle of water evaporation and condensation that creates rivers and lakes, and the biological cycles of photosynthesis and life. Covering 0.16% of the land on earth with 10% efficient solar conversion systems would provide 20 TW of power, nearly twice the world's consumption rate of fossil energy. These comparisons illustrate the impressive magnitude of the solar resource, providing an energy stream far more potent than present-day human technology can achieve. Solar energy is already being successfully used in residential and industrial settings for cooking, heating, cooling, lighting, space technology, and for communications among other uses. While the reserves of fossil fuels are restricted, there is no limitation to the availability of solar energy.

All routes for utilizing solar energy exploit the functional steps of capture, conversion, and storage. The sun's energy arrives on earth as radiation distributed across the color spectrum from IR to UV. The energy of this radiation must be captured as excited electron hole pairs in a semiconductor, a dye, or a chromophore, or as heat in a thermal storage medium. Excited electrons and holes can be tapped off for immediate conversion to electrical power, or transferred to biological or chemical molecules for conversion to fuel. Natural photosynthesis produces fuel in the form of sugars and other carbohydrates derived from the reduction of CO_2 in the atmosphere and

used to power the growth of plants. The plants themselves become available for as biomass for combustion as primary fuels or for conversion in reactors to secondary fuels like liquid ethanol or gaseous carbon monoxide, methane, and hydrogen. We are now learning to mimic the natural photosynthetic process in the laboratory using artificial molecular assemblies, where the excited electrons and holes can drive chemical reactions to produce fuels that link to our existing energy networks. Atmospheric CO_2 can be reduced to ethanol or methane, or water can be split to create hydrogen. These fuels are the storage media for solar energy, bridging the natural day-night, winter-summer, and cloudy-sunny cycles of solar radiation.

In addition to electric and chemical conversion routes, solar radiation can be converted to heat energy. Solar concentrators focus sunlight collected over a large area to a line or spot where heat is collected in an absorber. Temperatures as high as 3000°C can be generated to drive chemical reactions, or heat can be collected at lower temperatures and transferred to a thermal storage medium like water for distributed space heating or steam to drive an engine. Effective storage of solar energy as heat requires developing thermal storage media that accumulate heat efficiently during sunny periods and release heat slowly during dark or cloudy periods. Heat is one of the most versatile forms of energy, the common link in nearly all our energy networks. Solar thermal conversion can replace much of the heat now supplied by fossil fuel. Although many routes use solar energy to produce electricity, fuel, and heat, none are currently competitive with fossil fuels for a combination of cost, reliability, and performance.

2 Different technologies for harnessing solar energy

Technologies and resources are used to convert solar radiation into solar energy to store it or convert it for other applications and can be broadly classified into two groups: (1) photovoltaic (PV) *(7)* and (2) solar thermal *(8)*.

The PV technology converts radiant energy contained in light quanta into electrical energy when light falls upon a semiconductor material by causing electron excitation and strongly enhancing conductivity. Solar thermal technology uses solar heat, which can be used directly for either thermal or heating application or electricity generation. Accordingly, it can be divided into two categories: (1) solar thermal nonelectric and (2) solar thermal electric. The former includes applications such as agricultural drying, solar water heaters, solar air heaters, solar cooling systems, and solar cookers, and the latter refers to the use of solar heat to produce steam for electricity

generation, also known as concentrated solar power (CSP). In addition to the above technologies, of utilizing the solar energy spectrum, it is also important to check for the possibility of tailoring the spectral absorptance, emittance, reflectance, and transmittance of a surface to meet different demands in different wavelength intervals, that is, to take advantage of spectral selectivity of the solar grade materials *(9)*.

2.1 Solar PV technology

Solar power can be converted directly into electrical power in PV cells, commonly called solar cells. The sun has a surface temperature of about 6000°C, and its hot gases at this temperature emit light that has a spectrum ranging from the UV, through the visible, into the IR. According to quantum theory, light can behave either as waves or as particles, depending upon the specific interaction of light with matter; this phenomenon is called the wave-particle duality of light. In the particle description, light consists of discrete particle-like packets of energy called photons. Sunlight contains photons with energies that reflect the sun's surface temperature; in energy units of electron volts (eV), the solar photons range in energy ($h\nu$) from about 3.5 eV (UV region) to 0.5 eV (IR region). The energy of the visible region ranges from 3.0 eV (violet) to 1.8 eV (red); the peak power of the sun occurs in the yellow region of the visible region, at about 2.5 eV. At high noon on a cloudless day, the surface of the Earth receives 1000 W of solar power per square meter (1 kW/m^2).

PV cells generally consist of a light absorber that will only absorb solar photons above certain minimum photon energy. This minimum threshold energy is called the "energy gap" or "band gap" (Eg); photons with energies below the band gap pass through the absorber, while photons with energies above the band gap are absorbed. The light absorber in PV cells can be either inorganic semiconductors, organic molecular structures, or a combination of both. In inorganic semiconductor materials, such as Si, electrons (e^-) have energies that fall within certain energy ranges, called bands. The energy ranges, or bands, have energy gaps between them. The band containing electrons with the highest energies is called the valence band. The next band of possible electron energies is called the conduction band; the lowest electron energy in the conduction band is separated from the highest energy in the valence band by the band gap. When all the electrons in the absorber are in their lowest energy state, they fill up the valence band, and the conduction band is empty of electrons. This is the usual situation in the dark. When photons are absorbed, they transfer their energy to electrons in the filled valence band and promote these electrons to higher energy states

in the empty conduction band. There are no energy states between the valence and conduction bands, which is why this separation is called a band gap and why only photons with energies above the band gap can cause the transfer of electrons from the lower-energy-state valence band into the higher-energy-state conduction band. When photons transfer electrons across the band gap, they create negative charges in the conduction band and leave behind positive charges in the valence band; these positive charges are called holes (h+). Thus, absorbed photons in semiconductors create pairs of negative electrons and positive holes. In a PV cell, the electrons and holes formed upon absorption of light separate and move to opposite sides of the cell structure, where they are collected and pass through wires connected to the cell to produce a current and a voltage thus generating electrical power. The schematic is shown in Fig. 1.3.

2.2 Solar thermal technology

Solar thermal processes encompass a wide variety of technologies, all of which begin by converting the incident sunlight to heat. This heat can be converted to electricity, as is currently done in CSP plants via a Rankine or combined cycle *(10)*, solar thermoelectric generators (STEG) *(11)*, and solar thermophotovoltaics (STPV) [13,14]. Currently, there are 3 GW of installed and underconstructed CSP plants in the world, but STEGs and STPV have yet to be commercialized. Solar thermal energy, or the waste heat from the aforementioned solar-to electricity processes, can also be used for heating or cooling. Nearly 300 GW of solar thermal heat or hot water systems have been installed worldwide *(12)*.

A schematic of a typical solar thermal to electrical energy conversion system is shown in Fig. 1.4. In such solar thermal technologies, the sunlight is absorbed as heat at the absorber. This absorber must strongly absorb the sunlight, while ideally losing little heat to the environment via convection and radiation. An absorber, which has strong solar absorptance and low IR emittance, is called a spectrally selective absorber *(14,15)*.

Absorbers must efficiently convert a solar flux into heat and deliver that heat to the thermal system (Fig. 1.4). The efficiency of the conversion from solar irradiance at the absorber, H_{abs}, to a heat flux delivered to the thermal system, q_{h}, is defined as the absorber efficiency, η_{abs}:

$$\eta_{abs} = \frac{q_h}{H_{abs}} = \alpha_s - \varepsilon_t \frac{\sigma_{sb}\left(T_h^4 - T_{amb}^4\right)}{H_{abs}} - \frac{h_{conv}\left(T_h - T_{amb}\right)}{H_{abs}}$$

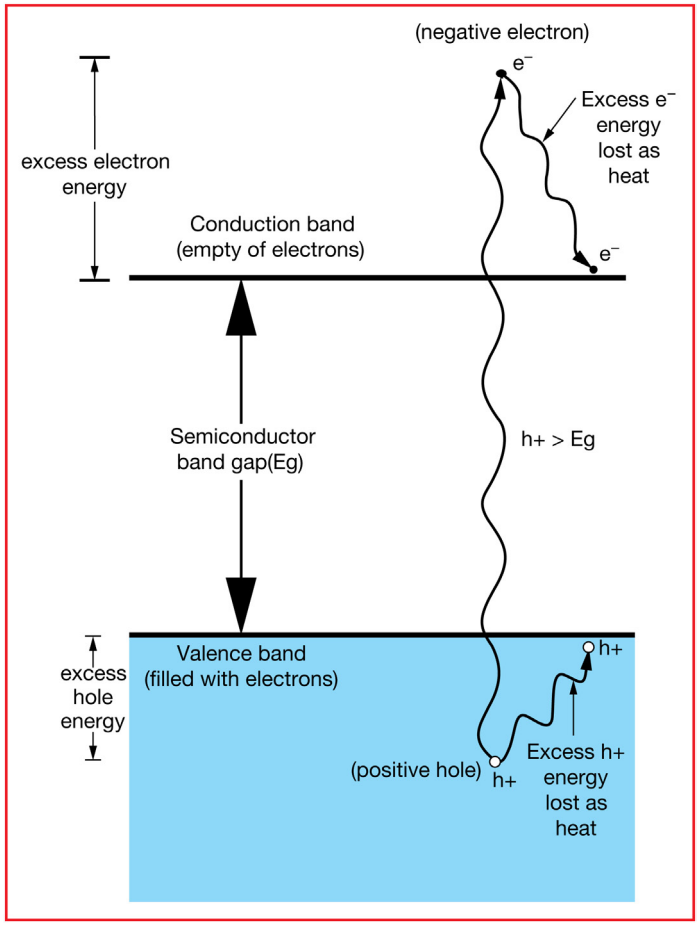

Figure 1.3 ***A diagram showing absorption of photon of energy*** (h_ν) ***greater than band gap of semiconducting materials.***

where σ_{sb} is the Stefan-Boltzmann constant, T_h is the absorber temperature, T_{amb} is the temperature of the environment, and h_{conv} is the convective heat transfer coefficient. The solar absorptance, α_s, is defined as:

$$\alpha_s = \frac{\int_0^\infty \int_0^{2\pi} \int_0^{\pi/2} \varepsilon'_\lambda(\lambda,\phi,\theta) S(\lambda,\phi,\theta) \cos\theta \sin\theta d\lambda \, d\phi \, d\theta}{\int_0^\infty \int_0^{2\pi} \int_0^{\pi/2} S(\lambda,\phi,\theta) \cos\theta \sin\theta d\lambda \, d\phi \, d\theta}$$

where λ is the wavelength of radiation, ϕ is the azimuthal angle, θ is the polar angle, ε'_λ is the spectral directional emittance at the operational temperature, and S is the incident solar intensity at the absorber. The numerator

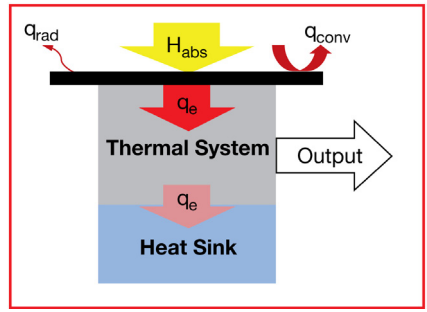

Figure 1.4 ***A typical solar thermal energy conversion system.*** Sunlight incident on the absorber (H_{abs}) is converted to a heat flux (q_h) and delivered to the thermal system, where the desired output (work, electricity, heat, cooling, etc.) is produced. Waste heat (q_c) may be generated in the process and rejected to a heat sink. Radiative (q_{rad}) and convective (q_{conv}) losses at the surface reduce the potential output of the system.

of this equation is the total absorbed solar energy; the denominator is the incident solar flux H_{abs}.

The thermal emittance, ε_t, is defined as:

$$\varepsilon_t = \frac{\int_0^{\infty}\int_0^{2\pi}\int_0^{\pi/2} \varepsilon'_{\lambda}(\lambda,\phi,\theta) I_{b\lambda}(\lambda,\phi,\theta)\cos\theta\sin\theta d\lambda\ d\phi\ d\theta}{\int_0^{\infty}\int_0^{2\pi}\int_0^{\pi/2} I_{b\lambda}(\lambda,\phi,\theta)\cos\theta\sin\theta d\lambda\ d\phi\ d\theta}$$

where $I_{b\lambda}$ is the blackbody intensity given by Planck's formula.

One of the efficient spectrally selective absorbers is a mixture of ceramics and metals (cermet). When integrated with an antireflection coating (ARC) and an IR-reflective base layer (either an intrinsically IR reflecting substrate or an IR-reflective coating on a substrate), cermet-based coatings (Fig. 1.5) can be very effective spectrally selective absorbers.

By having a large emittance in the solar wavelengths and a small emittance in the IR, absorbers can have high solar absorptance and low thermal emittance, thus resulting in high absorber efficiency. To maximize the absorber efficiency, multiple absorption mechanisms should be employed. One strategy is to explore new materials, including metal inclusions and dielectrics, which have high thermal stability and excellent optical properties for high temperature applications.

3 Interaction of matter with solar radiation

Rapid developments in nanoscience have created an unusual opportunity for advances in basic solar energy research. Because the individual microscopic steps of solar energy use take place on the nanometer scale, the ability

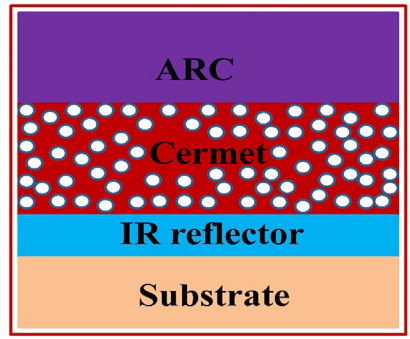

Figure 1.5 ***Schematic representation of a cermet-based spectrally selective absorber.*** The antireflection coating (ARC) reduces solar reflection off the surface; the cermet provides selective absorption; and the IR reflector (typically Cu, Al, Mo, or other metal with low intrinsic emissivity) reduces radiation losses. The substrate is usually metal (to conduct heat well) or glass (for lower cost). The cermet comprises a dielectric host (*dark red*) with metal particle inclusions (*circles*).

to pattern and control matter on this length scale presents unusual opportunities for researchers to create new materials for solar energy conversion and use. The emergence of new fundamental physical properties on this length scale could potentially lead to far more efficient technologies for conversion of solar energy to electricity and fuels. To take advantage of these new materials and processes, researchers must create complex arrangements of nanoscale components.

The most popular term in the nanoscale world is quantum confinement effect, which is essentially due to changes in the atomic structure as a result of direct influence of ultra-small length scale on the energy band structure *(16)*. The length scale corresponds to the regime of quantum confinement ranges from 1 to 25 nm for typical semiconductor groups of IV, III-V, and II-VI, in which the spatial extent of the electronic wave function is comparable with the particle size. As a result of these "geometrical" constraints, electrons "feel" the presence of the particle boundaries and respond to changes in particle size by adjusting their energy. This phenomenon is known as the quantum-size effect. Quantization effects become more important when the particle dimension of a semiconductor is near or below the bulk semiconductor Bohr exciton radius, which makes material's properties size dependent. In general, the Bohr radius of a particle is defined as *(17)*

$$r_b = \varepsilon \frac{m}{m^\star} a_0$$

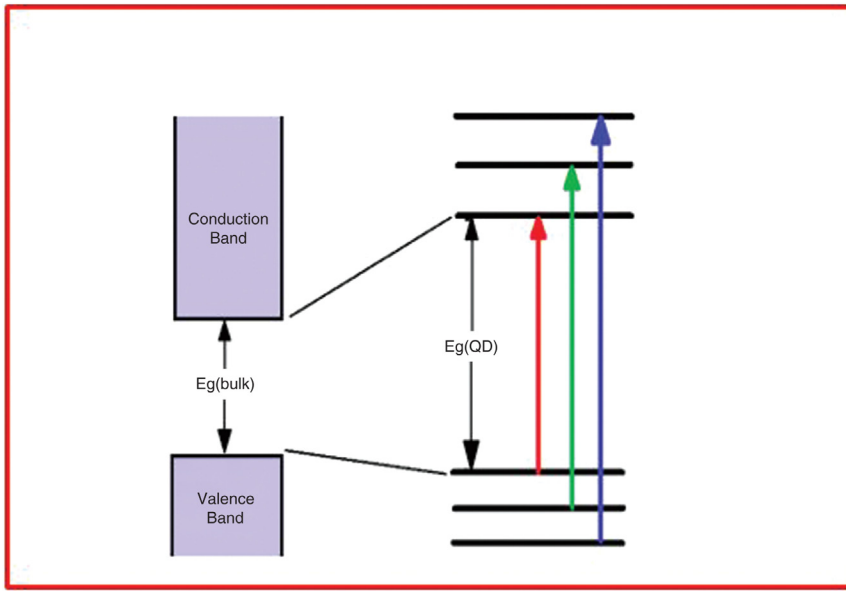

Figure 1.6 ***A schematic of the discrete energy level of a semiconductor.***

where ε is the dielectric constant of the material, $m^{\star}$ is the effective mass of the particle, m is the rest mass of the electron, and a_o is the Bohr radius of the hydrogen atom. When the particle size approaches Bohr exciton radius, the quantum confinement effect causes increasing of the excitonic transition energy and blue shift in the absorption and luminescence band gap energy *(17)*. For example, 4.8 nm diameter PbSe nano crystals (NCs) show an effective band gap of approximately 0.82 eV, exhibiting a strong confinement induced blue shift of >500 meV compared to the bulk PbSe band gap of 0.28 eV (the Bohr exciton radius in PbSe is 46 nm) *(18)*. In addition, quantum confinement leads to a collapse of the continuous energy bands of a bulk material into discrete, atomic like energy levels. The discrete structure of energy states leads to a discrete absorption spectrum, which is in contrast to the continuous absorption spectrum of a bulk semiconductor as shown in Fig. 1.6. A quantum confined structure is one in which the motion of the carriers (electron and hole) are confined in one or more directions by potential barriers. Based on the confinement direction, a quantum confined structure will be classified into three categories as quantum well, quantum wire, and quantum dots (QD) or nanocrystals. The basic type of quantum confined structure is given in Table 1.1.

Table 1.1 Classification of quantum confined structures.

Structure	Quantum confinement	Number of free dimension
Bulk	0	3
Quantum well/superlattices	1	2
Quantum wire	2	1
Quantum dot/nanocrystals	3	0

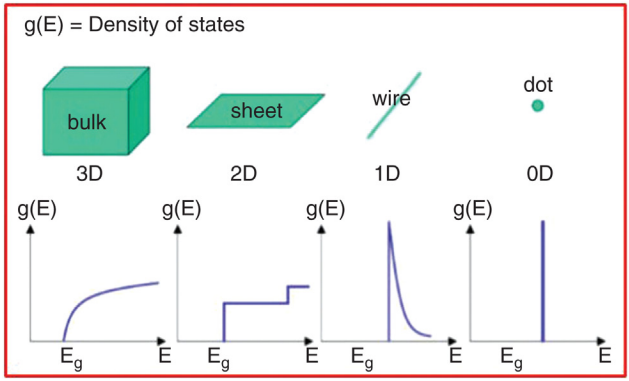

Figure 1.7 ***Density of electron states of a semiconductor as a function of dimension. The optical absorption spectrum is roughly proportional to the density of states.***

In QDs, the charge carriers are confined in all three dimensions which the electrons exhibit a discrete atomic-like energy spectrum. Quantum wires are formed when two dimensions of the system are confined. In quantum well, charge carriers (electrons and holes) are confined to move in a plane and are free to move in a two-dimensional. Also, the energy level of one of the quantum numbers changes from continuous to discrete. Compared with bulk semiconductors, the quantum well has a higher density of electronic states near the edges of the conduction and valence bands, and therefore a higher concentration of carriers can contribute to the band-edge emission. As more number of the dimension is confined, more discrete energy levels can be found; in other words, carrier movement is strongly confined in a given dimension. Density of electron states in bulk, 2D, 1D, and 0D semiconductor structures, are shown in Fig. 1.7. 0D structures have very well-defined and quantized energy levels. The quantum confinement effect corresponding to the size of the nanostructure can be estimated via a simple effective-mass approximation model.

This method can predict the confined energy levels of nanostructures by solving Schrodinger equation assuming the barriers have an infinite confining

potential. The "effective mass" solutions of the Schrödinger equation for electrons confined in a quantum dot or NCs, quantum wire and quantum well are: Quantum dot or nanocrystal:

$$E_{n,m,l} = \frac{n^2\hbar^2}{2m^\star}\left(\frac{n^2}{L_z^2}+\frac{m^2}{L_y^2}+\frac{l^2}{L_x^2}\right),= \phi(z)\phi(y)\phi(x)$$

Quantum wire:

$$E_{n,m}\left(k_x\right) = \frac{n^2\hbar^2}{2m^\star}\left(\frac{n^2}{L_z^2}+\frac{m^2}{L_y^2}\right)+\frac{\hbar^2k_x^2}{2m^\star},= \phi(z)\phi(y)\,exp\left(ik_x x\right)$$

Quantum well:

$$E_{n,m,l} = \frac{n^2\hbar^2n^2}{2m^\star L_z^2}+\frac{\hbar^2}{2m^\star}\left(k_x^2+k_y^2\right),= \phi(z)\,exp\left(ik_x x+ik_y y\right)$$

where $n, m, l = 1, 2 \ldots$ the quantum confinement numbers; L_x, L_y, and L_z are the confining dimensions; $\exp\left(ik_x x+ik_y y\right)$ is the wave function describing the electronic motion in x and y directions, similar to free electron wave functions.

In addition to the quantum confinement effect of nanostructures, their small dimensions, results into extremely large surface area to volume ratio, which makes a large number of surface or interfacial atoms, are resulting in more surface dependent properties. Nanomaterials can be classified depending on the dimensions such as (1) 0D spheres and clusters, (2) 1D nanofibers, nanowires, and nanorods, (3) 2D films, plates, and networks, (4) 3D nanomaterials and is shown in Fig. 1.8. While most of micro structured materials have similar properties to the corresponding bulk materials, the

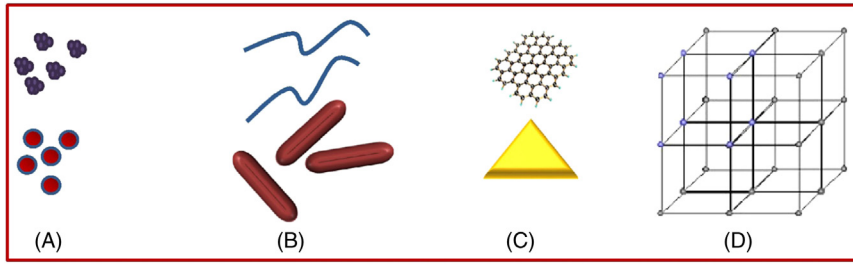

Figure 1.8 Classification of nanomaterials (A) 0D spheres and clusters, (B) 1D nanofibers, wires, and rods, (C) 2D films and networks, (D) 3D nanomaterials.

properties of materials with nanometer dimensions are significantly different from those of atoms and bulk materials. This is mainly due to the nanometer size of the materials, which render them: (1) large fraction of surface atoms, (2) high surface energy, (3) spatial confinement, and (4) reduced imperfections cannot be seen exist in the corresponding bulk materials *(19)*. Reduced imperfections are also an important factor in the determination of the properties of the nanomaterials.

4 Effect of nanostructuring on the solar energy harvesting

Due to these changes in the properties of nanoparticles as compared to their bulk counterparts, Nanostructure-based solar energy is attracting significant attention as a possible candidate for achieving drastic improvement in the field of solar energy conversion to some useful applications *(20)*. To improve the efficiency of solar energy conversion technologies, we have to increase the absorbance of the materials; this can be achieved by taking that material into the nano scale range because due to change in size, the band gap and density of states also change. So, we can use nanostructured layers instead of traditional thin-film solar cells. Nanostructured layers in thin-film solar cells offer three important advantages. First, due to multiple reflections, the effective optical path for absorption is much larger than the actual film thickness. Second, light-generated electrons and holes need to travel over a much shorter path and thus recombination losses are greatly reduced. As a result, the absorber layer thickness in nanostructured solar cells can be as thin as 150 nm instead of several micrometers in the traditional thin film solar cells. Third, the energy band gap of various layers can be made to the desired design value by varying the size of nanoparticles. This allows for more design flexibility in the absorber of solar cells. Examples to this type of layers are: polycrystalline thin-film solar cells such as $CuInSe_2$ (CIS), $Cu(In,Ga)Se_2$ (CIGS), and CdTe compound semiconductors *(21,22)*. Because of the high absorption coefficient ($\sim 10^5$ cm^{-1}), a thin layer of ~2 mm is sufficient to absorb the useful part of the spectrum. Fig. 1.9 shows the schematic structure of CIGS-based solar cells obtained by low-temperature pulsed electron deposition, with the experimentally achieved efficiency of 15% *(23)*.

Moreover, nanomaterials are smaller in size and also have lightweight; due to this, lightweight and flexible solar cells can yield a high specific power (W/kg) and open numerous possibilities for a variety of applications. Interaction of solar radiations with matter at nanoscale has two advantages;

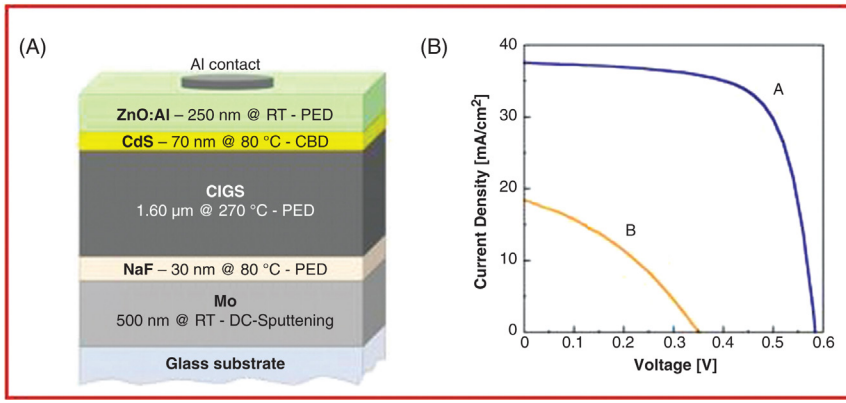

Figure 1.9 (A) Schematic diagram of CIGS photovoltaic (PV) structure. (B) ($I - V$) Characteristic for the CIGS solar cell. Source: (23) *Copyright.*

it improves light absorption and reduces the amount of material needed. Another advantage of nanoscale is that some of the indirect band gap semiconductors can be transferred to strongly absorbing direct band gap semiconductors and can be used as a thin film solar cells such as silicon, which has mostly dominated the PV industry.

As we know, electromagnetic radiation (primarily in the visible and near-infrared regions of the spectrum) is emitted from the sun and absorbed by the solar cell. A photon will then excite a negatively charged electron from the valence band (low energy state) to the conduction band (a higher energy state) leaving behind a positively charged vacancy, called a hole. For this energy transfer to create any usable energy, the photon must have energy greater than the bandgap of the material, or else the electron will immediately relax down and recombine with the hole and the energy will be lost as heat. Upon excitation above the bandgap, the photon creates an electron and a hole, which are now free to move throughout the semiconductor crystal. These act as charge carriers, which transport the energy to the electrical contacts, which results in a measurable external current. Current solar cells cannot convert all the incoming light into usable energy because some of the light can escape back out of the cell into the air. Additionally, sunlight comes in a variety of colors and the cell might be more efficient at converting bluish light while being less efficient at converting reddish light. Higher energy light does excite electrons to the conduction band, but any energy beyond the band gap energy is lost as heat. All these problems can be resolved by using the QDs instead of the bulk materials *(24)*. The access energy, which is lost in the form of heat after excitation of

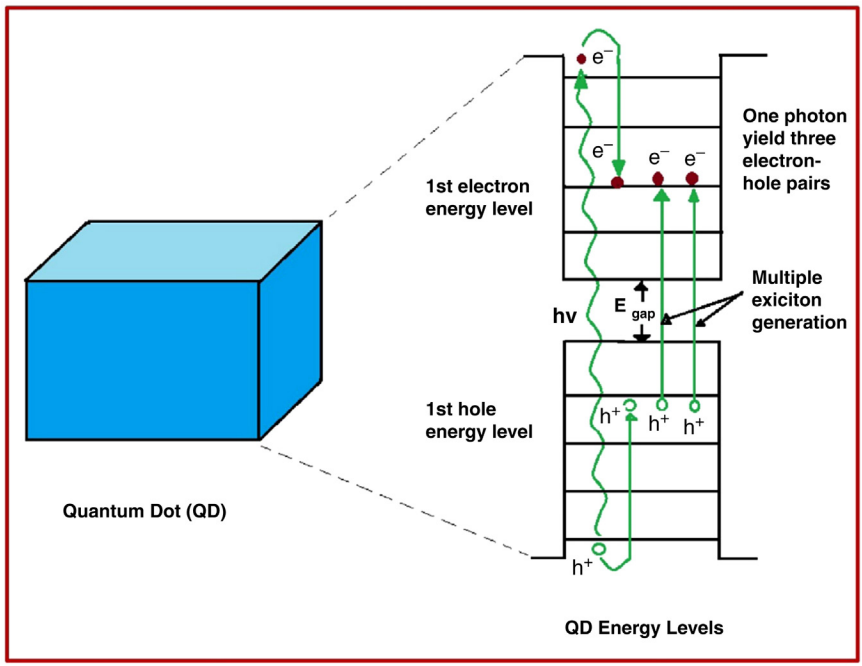

Figure 1.10 ***Multiple exciton generation in quantum dots.*** Because of quantum confinement in the small nanoscale semiconductor QD particle, the energy levels for electrons and holes are discrete. This slows hot exciton cooling and enhances multiple exciton formation. A single absorbed photon that has energy at least 3 times the energy difference between the first energy levels for electron and holes in the QD can create 3 excitons. The bandgap of the bulk semiconductor is indicated as Eg.

electron, is further used in QDs for multiple exciton generation as shown in the schematic given in Fig. 1.10 *(25,26)*.

In bulk semiconductors, this process is known as electron hole pair multiplication (EHMP) and occurs when more than one electron hole pair is produced by absorption of one photon of energy at least twice the band gap. Nozik et al. reported that production of these electron-hole pair increases by ~2 in PbSe QDs compared to bulk PbSe. EHMP is more efficient in PbSe QDs than in bulk PbSe *(29)*. It is reported that in QDs there are at least three fundamental properties that are modified due to quantum confinement and affect the EHPM process. (A) Crystal momentum is no longer a good quantum number. There are three factors that can affect $h\nu_{th}$ (threshold energy) related to crystal momentum: (1) absorption selection rules are modified; (2) conservation of crystal translational momentum is relaxed, allowing $h\nu_{th}$ to be less than that required by momentum conservation. In fact, we find $h\nu_{th}$ in QDs of PbSe is lower than that allowed by

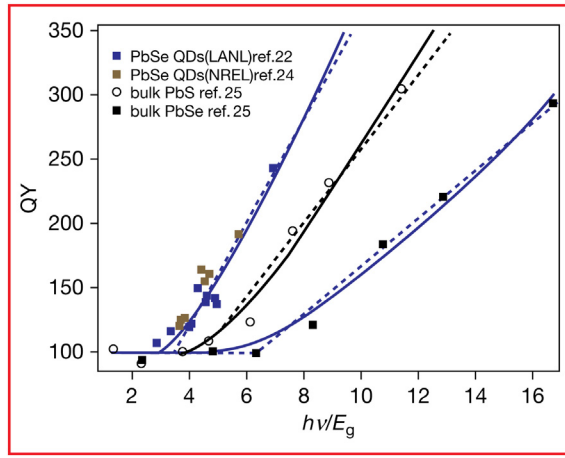

Figure 1.11 ***QY vs. hν/Eg for PbSe QD, PbSe bulk, and PbS bulk samples.*** Source: *[29–31] Copyright.*

momentum conservation in bulk PbSe, and (3) single- and multiexcitonic states can be coupled through the Coulomb operator to form a superposition of states. Such coupling is not possible in bulk systems with well-defined momentum. The best way to compare EHPM processes between semiconductor QDs and bulk semiconductors is to plot the quantum yield (QY) vs. $h\nu$/Eg (threshold energy needed to produce extra electron-hole pair) as this provides a direct determination of the EHPM efficiency, η_{EHPM}, and allows for determination of the relative contributions of EHPM and competing relaxation channels and is shown in Fig. 1.11 for PbSe QD and PbSe and PbS bulk samples. (B) The discrete structure of semiconductor QD energy bands, due to quantum confinement and intimate control over surface states and surface ligands, can be used to modify carrier relaxation rates. (C) Increased Columbic coupling between excitons in QDs increases Auger-related processes like multiple-exciton-generation (MEG).

Due to these properties of QDs, solar cells produced from QDs can have much higher power conversion efficiencies than their bulk counterparts and are given in Fig. 1.12. The results are based on Shockley-Queisser (SQ) detailed balance calculations given [I]. In Fig. 1.12, curve 6 (black solid line) is the conventional SQ (Shockley-Queisser) calculation with just 1 EHP created per photon at the band gap; curve 1 (solid red curve) assumes the maximum multiplication energetically allowed and is based on M_{max}. Curve 2 (solid green line) is based on $h\nu_{th}$ = 2Eg followed by creation of one extra exciton created per Eg (defined as the L2 characteristic); curve 3 (solid blue

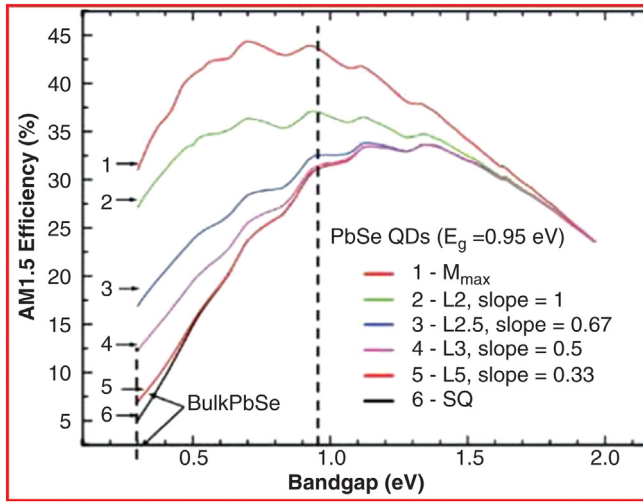

Figure 1.12 ***PV power conversion efficiencies at AM1.5 vs. band gap for various characteristics of MEG QY.*** Source*:* (29) *Copyright.*

line) is based on a threshold of 2.5 Eg, curve 4 is based on a threshold of 3Eg (defined as the L3 characteristic); curve 5 is based on a threshold of 4.5Eg with η_{EHPM} 0.19 (defined as the L5 characteristic and is the experimental bulk characteristic for PbSe *(29)*.

As seen in this Fig. 1.12, the maximum thermodynamic conversion efficiency of ~5% for bulk PbSe is only marginally enhanced when the experimentally measured EHPM is included. Thus, EHPM in bulk PbSe cannot produce a significant enhancement of conversion efficiency. In contrast, for PbSe QDs with a quantized band gap of 0.95 eV, the maximum thermodynamic conversion efficiency is 31% for the SQ calculation, 37% for the L2 characteristic (solid green line), 32% for the L3 characteristic (solid purple line), and 42% for the M_{max} characteristic (solid red line). These calculations show that PbSe QDs will always have a much higher theoretical conversion efficiency compared to bulk PbSe (by factors ranging from 2.7 (L3 characteristic) to 3.5 (M_{max} characteristic) *(29,30)*.

5 Importance of solar thermal technology

Another aspect of using the incoming solar photon is photo thermal energy production, and to look for new technologies to efficient conversion of solar energy into electricity, it has become much important to look for several ways of minimizing energy utilization, as conservation of energy is the most

effective way of reducing CO_2 concentration, which has risen from ~315 ppm at the end of the 1950s so that it now exceeds ~400 ppm, without any sight for this reduction. In view of this, it becomes important to reduce the usage of fossil fuels and also the electricity usage, which reduces the harmful effect of CO_2 emission, that is, global warming, by making energy efficient building, windows, and vehicle. In this direction, it becomes very important to study a unique class of materials called as solar energy materials, for thermal applications and have optical properties that make them well adapted for utilizing solar energy and for reaching energy efficiency, especially in the built environment *(31)*. As we know that electricity utilization in-house and industrial is must. For example, in the United States, air conditioning-based in-house cooling consumes ~15% of the primary energy used by buildings.

Solar energy materials have properties that are tailored to the characteristics of the electromagnetic radiation in our natural surroundings, especially its spectral distribution, angle of incidence, and intensity. This tailoring can be made with regard to solar irradiation, thermal emission, atmospheric absorption, VIS, photosynthetic efficiency, and more. Solar energy materials can be of many kinds, for example, metallic, semiconducting, dielectric, glassy, polymeric, gaseous, etc. In particular, thin surface coatings of solar energy materials may exhibit the desired properties in their own right or may yield such properties when backed by an appropriate substrate. By using these smart solar energy materials for strategically cooling or heating, which keeps indoor comfort without electricity requirement, will therefore impact the global energy consumption *(32)*. Energy-efficient window is therefore considered to be the first step for reducing energy consumption through the reduction of heat transfer between indoor and outside environments. Windows are the key components to any building's design and provide the strategy to improve energy efficiency of the building. The conventional glass windows without any coatings films allow the passage of visible transmittance as well as solar heat that in turn increase the heating as well as cooling of the building structure. However, a functional coating on the glass eliminates solar heat and reduces the energy consumption. The functional materials and energy efficient windows have become a subject of intensive study toward energy conservation that has been discussed aplenty *(33–53)*.

There are a variety of coating technologies such as thermo-chromic, low-emission (low-e) coating, aerogel, photochromic, electrochromic, gasochromic, suspended particle, and liquid crystal that are demonstrated for energy saving windows application. Fig. 1.13 shows the passive IR regulating coating for smart windows application. As shown in Fig. 1.13 above,

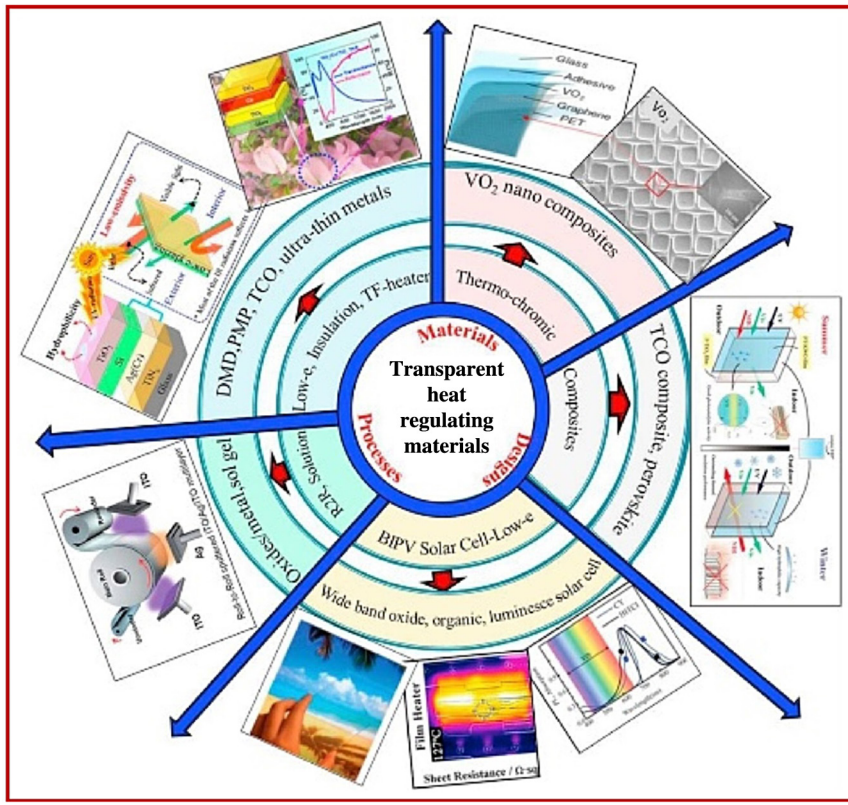

Figure 1.13 ***Schematic diagram of transparent heat regulating (THR) materials, multi-layer coating, and applications.*** Source*: [56–63] Copyright.*

the thermochromic coating of metal oxides on the window glass of the building can be used for reducing the energy loss by controlling the heat flow across them. Thermo-chromic materials are capable of changing their optical properties when exposed to heat. The transmittance and reflectance can be significantly altered due to phase transition; in common language, there is a change in the color of the materials coating due to influence of thermal energy. The performance of thermo-chromic materials can be evaluated by phase transition temperature (T_c), luminous transmittance (T_{lum}), visible transmittance, and modulation capability of solar energy (ΔT_{sol}). The transition temperature represents the critical value of temperature beyond which the thermo-chromic materials change its phase from semiconducting to metallic or shows change in color *(35)*. The energy saving efficiency of thermo-chromic coating can be estimated by the change in transmittance of the coating at 2500 nm before and after metal to semiconductor transition temperature; that is called switching efficiency *(62)*. The ratio of

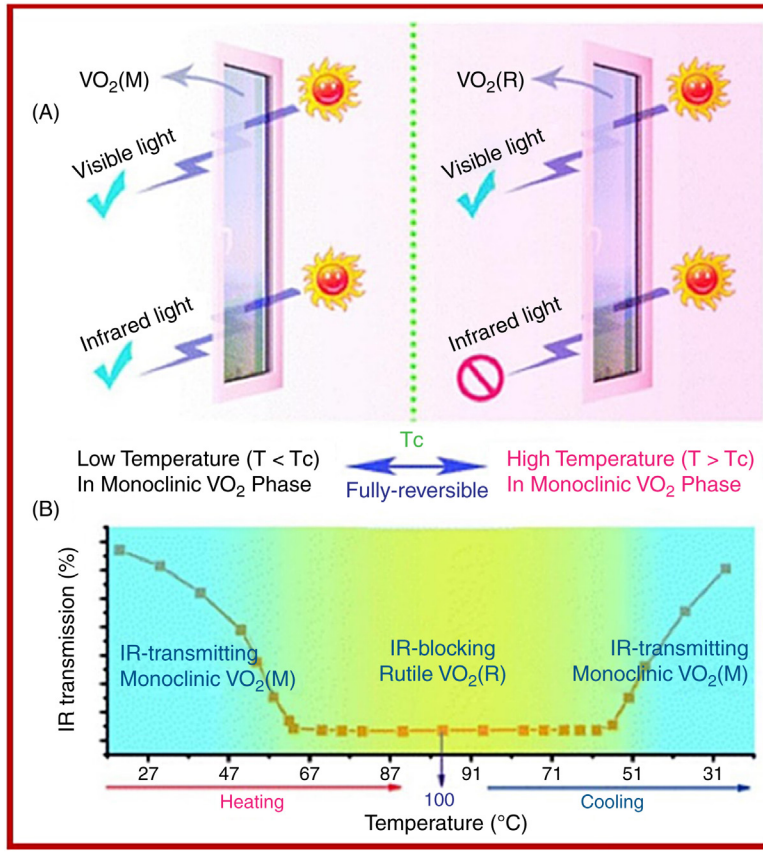

Figure 1.14 (A) Schematic of visible and infrared light transmission from VO2 film at low and high temperature corresponds to insulator to metallic phases. (B) IR transmittance profile of VO2 film during heating and cooling. Source: (61) *Copyright.*

transmitted light to incident light is defined as luminous transmittance and presented as % of light transmitted. The transmittance of solar energy before and after transition is measured by the solar modulation efficiency (ΔT_{sol}) *(35)*. Among the various transition metal oxides (lower oxides of vanadium, titanium, iron, and niobium), thermo-chromic properties of VO_2 are extensively investigated due to lower transition temperature and sharp transition features. Thermo-chromic properties in transition metal oxide appear due to d-d transitions with shift in Fermi level under thermal excitation and lattice expansion and temperature-dependent electron-phonon coupling *(63)*. Insulator-to-metal transition at 68°C in vanadium dioxide (VO_2) is responsible for electrochromic behavior. Fig. 1.14 shows the schematic diagram for insulator to metal transition of VO_2 and its impact in optical

properties. Numerous efforts have been reported to improve the thermochromic properties of VO_2 materials especially to reduce the T_c to make the technology disruptive for commercial utilization. It has been found that the doping of VO_2 by numerous foreign cations (W^{6+}, Nb^{5+}, Ti^{4+}, Cr^{3+}, or Al^{3+}) is reported, and it is noticed that doping changes the transition temperature considerably *(64)*.

The conventional glass emits 84% of the radiant heat falling upon it by absorbing and transmitting IR radiation while reflecting only 16% of IR radiation *(65)*. Transparent heat reflector reflects IR of wavelength ($k > 700$ nm) and allows the transmission of VIS with 400 nm $< k <$ 700 nm *(33,85)*. Harmful UV radiation is normally absorbed by the glass substrate or dielectric layers within the structure. The dielectric/metal *(66)* and dielectric/metal/dielectric-based multilayers *(33,38–41,42,44,50,54,67,68,69–73)* with low emission (low-e) materials act as heat reflecting coatings. Low-thermal emittance (low-e) coatings effectively reduce IR radiation transfer through windows, which reduces thermal leakage from indoors to the outdoor surroundings. It consists of thin metal to protect metal layer from the environment and also acts as antireflecting coating to increase visible transmission through the coating layer *(54,74)*. The undercoat layer improves adhesion between glass and metal layer *(48,68)*. Design of dielectric layer based on metal oxides and sulfide is very crucial as it enhances visible transmission without reducing IR reflection and protects coating from the harsh ambient *(43,52,54,75–78)*. Microstructural properties of thin metal layer and dielectric passivation layers have significant roles on the IR reflectance and visible transmittance *(45–47,79)*. Growth mechanism and choice of interfacial layer enhance the stability and durability of the coating *(39,45,48,50,77,80–83)*. Apart from presenting the desirable optical performance, commercial transparent heat reflector coating is designed to be chemically, thermally, and mechanically stable.

Low-e coating can be divided into two categories; high solar gain low-e and low solar gain low-e, as shown in Fig. 1.15. The high solar gain low-e coating is more suitable for cold weather, as it allows visible transmission and near infra-red (NIR) into the building, whereas, low solar gain low-e is suitable for hot weather since the latter reflects NIR into the atmosphere and keeps the building cool. By choosing appropriate materials and multilayer structure, optical performance of the coating can be tuned. Thickness of dielectric and metal plays important role to develop low solar gain low-e and high solar gain low-e *(46,49,52,54,74,84–86)*. Furthermore, optical properties (visible transmittance and IR reflectance) of the multilayer

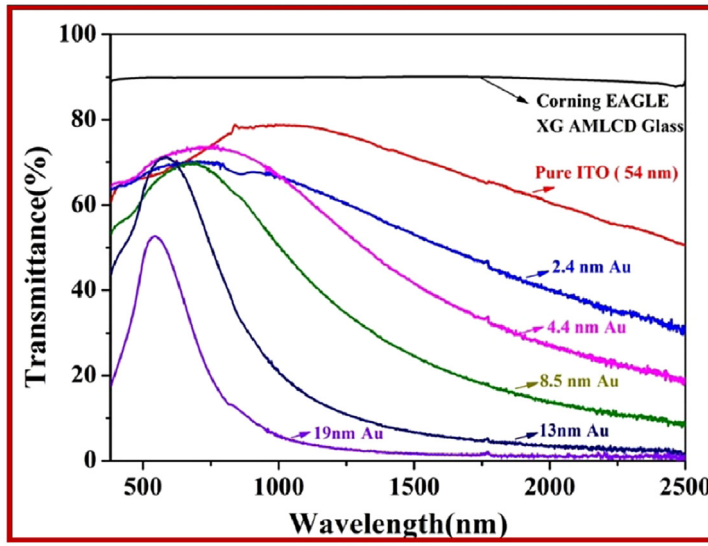

Figure 1.15 ***Direct spectral transmittance of trilayered samples (ITO/Au/ITO) with different gold spacer thicknesses.*** Source: *(91) Copyright.*

depend on the synthesis process, microstructural property, interface engineering, and design of the multilayers *(43,51–53,75,72,76-78,87–90)*.

6 Novel materials for regulating IR radiation

Besides low-e and thermo-chromic materials, transparent solar cells on glass/plastic substrates are emerging rapidly for building-integrated photovoltaics (BIPV) for energy-harvesting windows. The transparent solar cell is capable of generating electricity while simultaneously reducing heating and cooling demands for indoor comfort. Transparent solar cells with heat mirror can empower the solar energy harvesting and reduces the electricity consumption required for indoor comfort *(92)*. Inorganic and organic semiconductors have been employed for transparent/semitransparent solar cells *(92–94)*. Semitransparent perovskite solar cells (PSCs) are not only highly efficient but also very effective in thermal-mirror operation. The average power conversion efficiency of semitransparent PSCs is 13.3% and the outstanding NIR rejection is ~85.5%. This demonstrates their great potential for ideal "energy generating and heat-rejecting" solar window applications making smart use of solar energy. In addition, dye-sensitized solar cells (DSSCs) and organic lead halide PSCs have attracted significant attention as next-generation low-cost photo-voltaics because of the potential

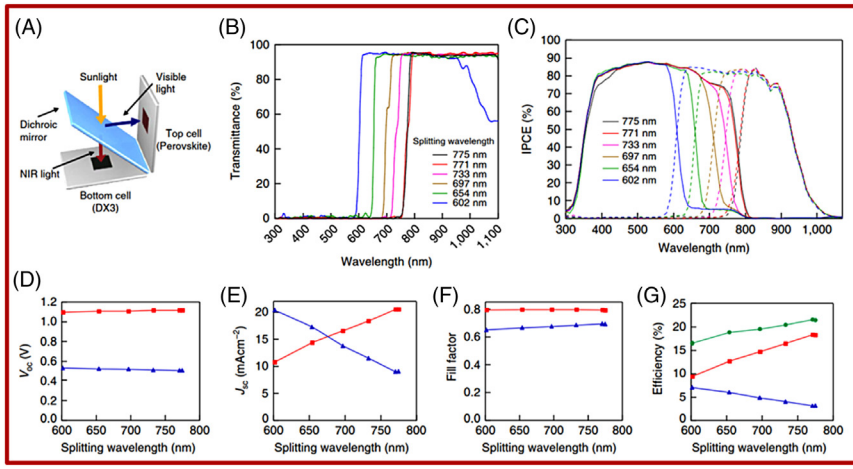

Figure 1.16 ***Device structure, IPCE spectra, and J-V characteristics of the hybridized cell.*** (A) Device structure of the hybridized cell using a dichroic spectrum splitter. (B) Transmittance spectra of dichroic mirrors under measurement conditions such as incident of a 45° angle. (C) IPCE spectra of the individual components of the hybridized cell with various dichroic mirrors: visible absorbing cell, PSC (*solid line*); near-IR absorbing cell, DX3-based DSSC (*dashed line*). (D-G) PV parameter and total power conversion efficiency dependence on the splitting wavelength of the dichroic mirrors: PSC (*red*), DX3-based DSSC (*blue*), and total power conversion efficiency of the hybridized cell (*green*). Source*:* (93) *Copyright.*

widespread applications. Fig. 1.16 shows below a hybridized solar cell employing a spectral splitting system, which was constructed using dichroic mirrors at an angle of 45° with splitting edge wavelengths of 602, 654, 697, 733, 771, and 775 nm. It can be seen that by using series connection, the light absorption band can be adjusted so as to equal the photocurrent of each component under standard sunlight. In this, a high-voltage PSC with a lead bromide perovskite will show the high-energy bandgap (B 2.3 eV), and therefore the series-connected tandem cell would achieve up to 22% PCE.

Transparent polymer solar cells selectively absorb solar spectrum and convert into electricity *(94–98)*. All solution-based transparent solar cells with novel materials are ideal to regulate NIR for smart windows application *(92,93,98)*. Luminescent materials-based fully transparent solar cells not only reduce IR transmittance into the building but also convert NIR into electricity *(61,99)*.The near-infrared transparent luminescent solar cells (TLSCs) based on organic salts provide an alternative strategy for transparent solar harvesting systems that can ultimately enhance the overall system efficiency of combined UV and NIR TLSCs. As shown in Fig. 1.17. Lunt et al. have designed and fabricated the first visibly transparent luminescent

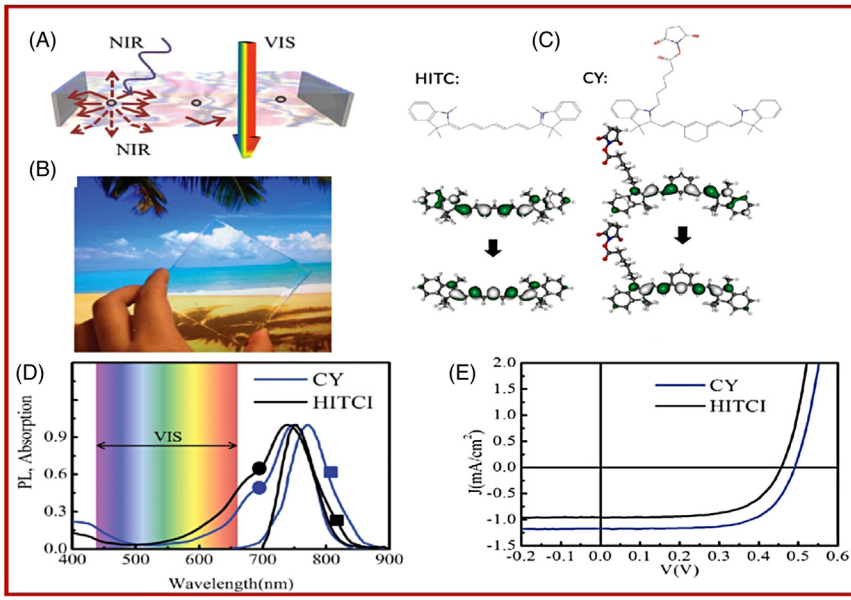

Figure 1.17 (A) Schematic of the transparent luminescent solar concentrator. (B) Photograph of the transparent LSC system incorporating CY luminophore. (C) CY and HITC molecular cation structures (*top*); the natural excited-state transition orbital pairs for HITC (*left*) and CY (*right*). The hole orbitals are shown on the top of the excited electron orbitals. Two cyanine derivatives: 2-[7-(1,3-dihydro-1,3,3-trimethyl-2H-indol-2-ylidene)-1,3,5-heptatrienyl]-1,3,3-trimethyl3H-indolium (HITC) iodide (HITCI) and 1-(6-(2,5-dioxopyrrolidin-1-yloxy)-6-oxohexyl)-3,3-dimethyl-2-((E)-2-((E)-3-((E)-2-(1,3, trimethylindolin-2ylidene)ethylidene) cyclohex-1-enyl)vinyl)-3H-indolium chloride (CY) have been used for the TLSCs. (D) Normalized absorption (*circle symbols*) and emission (*square symbols*) spectra of the NIR-absorbing luminophores CY (*blue line*) and HITCI (*black line*) films. (E) Current density as a function of voltage for the fully assembled TLSC systems with two of the luminophores. Source*:* (61) *Copyright*.

solar concentrator devices, which selectively harvest NIR photons based on fluorescent organic salts. These transparent TLSCs exhibit a nontinted transparency of 86 ± 1% in the visible spectrum combined with an efficiency of 0.4 ± 0.03% and have the potential for efficiencies up to 10% due to the large fraction of photon flux in the near-infrared *(61)*. These transparent NIR LSCs provide a new route to transparent light-harvesting systems with tremendous potential for high defect tolerances and processability. Vasiliev et al. demonstrated a new class of solar window system ready for industrial application *(77)*. UV and IR radiation energy are converted and/or deflected geometrically toward the panel edge for collection by copper-indium selenide ($CuInSe_2$)-based solar cells. The power conversion efficiencies 3.04%

in 10 cm × 10 cm vertically placed clear glass panels facing direct sunlight, and up to 2.08% in 50 cm × 50 cm installation ready framed window systems were demonstrated. Davy et al. demonstrated near-ultraviolet solar cells with electro-chromic windows for smart management of the solar spectrum *(99)*. Single-junction organic solar cells integrating with a low-cost, polymer-based electro-chromic window enables intelligent management of the solar spectrum *(99)*. Hence, we can say that for the economic commercial utilities, multifunctional performance of coatings is essential to enhance the energy conversion from the incoming solar radiation.

7 Conclusions

This chapter gives us the insight of technologies available for harnessing the huge amount of incoming solar radiation for its successful conversion into energy and hence can be treated as alternative to traditional fossil fuel-based sources of energy. It was discussed that using nanostructured materials having specific physical and chemical properties will lead to improvement in the efficiency of existing solar PV cell industry. In addition, the outcome from the chapter comes out to be that the use of spectrally selective coating over the windows/glass of the building can be used for regulating the heating and cooling of the inside environment. This type of functional coating on the glass eliminates solar heat and reduces the energy consumption, which will lead to energy saving, and will further tackle the CO_2 emission globally. Further, the plastic/glass-based transparent solar cells integrated with dielectric/metal/dielectric-based transparent conductor have been shown to empower the heat mirror and solar electricity for smart windows applications. This chapter, in turn, describes how incorporation of nanotechnology can improve the efficiency of solar energy conservation. One thing should be clear from this chapter: that solar energy and related materials research represents a dynamic field, whose importance and industrial viability are bound to increase in the future.

References

1. Bitran, M.; Murray, W. Infrared, Visible, and Ultraviolet Radiation. In *Patty's Toxicology*. John Wiley & Sons, Inc.: New York, 2001.
2. Poole, C. P., Jr.; Owens, F. J. *Introduction to Nanotechnology* John Wiley & Sons, Inc.: Hoboken, New Jersey, 2003.
3. Elliott, D. A.; Holland, J. M. Oral, Head, Neck Oncology, Reconstructive Surgery. In *Electromagnetic waves*; Zhurbenko, V., Ed.; BoD–Books on Demand: Denmark, 2018.
4. Granqvist, C. G., Ed. *Materials Science for Solar Energy Conversion Systems*; Pergamon: Oxford, UK, 1991.

5. Granqvist, CG Transparent Conductors as Solar Energy Materials: A Panoramic Review. *Sol. Energy Mater. Sol. Cells* **2007**, *91*, 1529–1598.
6. Hans, Kangro, Ed. *Planck's Original Papers in Quantum Physics*Taylor & Francis Ltd: London, 1972.
7. Archer, M. D., Hill, R., Eds. *Clean Electricity from Photovoltaics: Volume 1 of Series on Photoconversion of Solar Energy*Imperial College Press: London, UK, 2003.
8. Sangadevan, S. Recent Trends on Nanostructures Based Solar Energy Applications a Review. *Adv. Mater. Sci.* **2013**, *34*, 44–61.
9. Granqvist, C. G. Radiative heating and cooling with spectrally selective surfaces. *Appl. Opt., Optic. Soc. Am.* **1981**, *20* (15), 2606–2615.
10. Mills, D. Advances in solar thermal electricity technology. *Sol Energy* **2004**, *76*, 19–31.
11. Kraemer, D.; Poudel, B.; Feng, H. P.; Caylor, J. C.;Yu, B.;Yan, X., et al. High-performance flat-panel solar thermoelectric generators with high thermal concentration. *Nat. Mater.* **2011**, *10*, 532–538.
12. Mauthner, F.; Weiss, W. *Markets and Contribution to the Energy Supply 2011* Solar Heating & Cooling Programme, International Energy Agency: Paris, 2013.
13. Wang, N.; Han, L.; He, H. C.; Park, N. H.; Koumoto, K. A novel high-performance photovoltaic-thermoelectric hybrid device. *Energ Environ. Sci.* **2011**, *4*, 3676–3679.
14. Kennedy, C. E. *Review of Mid- to High-Temperature Solar Selective Absorber Materials* National Renewable Energy Laboratory: United States, 2002.
15. Niklasson, G. A.; Granqvist, C. G. Surfaces for selective absorption of solar energy: an annotated bibliography 1955-1981. *J. Mater. Sci.* **1983**, *18*, 3475–3534.
16. Wise, F.W. Lead salt quantum dots: The limit of strong quantum confinement. *Acc Chem Res* **2000**, *33* (11), 773–780.
17. YOFFE, A. D. Low-Dimensional Systems: Quantum Size Effects and Electronic Properties of Semiconductor Microcrystallites (Zero-Dimensional Systems) and Some Quasi-Two-Dimensional Systems. *Adv. Phys.* **1993**, *42* (2), 173–266.
18. Wise, F.W. Department of Applied Physics, Cornell University; Lead Salt Quantum Dots: the Limit of Strong Quantum Confinement. *Acc. Chem. Res.* **2000**, *33*, 773–780.
19. Corkish, R.; Kettemann, S.; Nelson, J. Low-Dimensional Systems and Nanostructures. *Phys. E* **April 2002**, *14* (1-2).
20. Corkish, R.; Kettemann, S.; Nelson, J. Proceedings of the Workshop on Nanostructures in Photovoltaics. Max Planck Institute for the Physics of Complex Systems, Dresden, Germany, July 28-4 August, 2001.
21. Ramanathan, K.; Contreras, M. A.; Perkins, C. L., et al. Properties of 19.2% efficiency ZnO/CdS/CuInGaSe2 thin-film solar cells. *Prog Photovolt: Res. Appl.* **1999**, *11*, 225.
22. Wu, X.; Kane, J.C.; Dhere, R.G.; DeHart, C.; Albin, D.S.; Duda, A.; Gessert, T.A.; Asher, S.; Levi, D.H.; Sheldon, P. In Proceedings of the 17th European Photovoltaic Solar Energy Conference and Exhibition, Munich, 2002, p. 995.
23. Rampino, S.; Armani, N.; Bissoli, F., et al. 15% Efficient Cu(In,Ga)Se2 Solar Cells Obtained by Low-Temperature Pulsed Electron Deposition. *Appl. Phys. Lett.* **2012**, *101* (132107).
24. Yoon, W.; Boercker, J. E.; Lumb, M. P.; Placencia, D.; Foos, E. E.; Tischler, J. G. Enhanced Open-Circuit Voltage of PbS Nanocrystal Quantum Dot Solar Cells. *Sci Rep* **2013**, *3*, 2225.
25. Yun, D.; Feng, W.; Wu, H.; Yoshino, K.; Efficient Conjugated Polymer-ZnSe and -PbSe Nanocrystals Hybrid Photovoltaic Cells Through Full Solar Spectrum Utilization. *Sol Energy Mater Sol Cells* **n.d.,** *93*, 1208-1213.
26. Schaller, Richard D., Melissa A. Petruska, and Victor I. Klimov. Effect of electronic structure on carrier multiplication efficiency: Comparative study of PbSe and CdSe nanocrystals. *Appl. Phys. Lett.* **87** (25), 2005, 253102.
27. Midgett, A. G.; Hillhouse, H. W.; Hughes, B. K.; Nozik, A. J.; Beard, M. C. Flowing versus static conditions for measuring multiple exciton generation in PbSe quantum dots. *J Phys Chem C* **2010**, *114* (41), 17486–17500.

28. Pijpers, J. J. H.; Ulbricht, R.; Tielrooij, K. J.; Osherov, A.; Golan, Y.; Delerue, C., et al. Assessment of Carrier-Multiplication Efficiency in Bulk PbSe and PbS. *Nat. Phys.* **2009**, *5*, 811–814.
29. Beard, M. C.; Midgett, A. G.; Hanna, M. C.; Luther, J. M.; Hughes, B. K.; Nozik, A. J. Comparing Multiple Exciton Generation in Quantum Dots to Impact Ionization in Bulk Semiconductors: Implications for Enhancement of Solar Energy Conversion. *Nano Lett* **2010**, *10*, 3019–3027.
30. Klimov, V. I. Detailed-Balance Power Conversion Limits of Nanocrystal-Quantum-Dot Solar Cells in the Presence of Carrier Multiplication. *Appl. Phys. Lett.* **2006**, *89*, 123118.
31. Granqvist, C. G.; Wittwer, V. Materials for Solar Energy Conversion: An Overview. *Sol. Energy Mater. Sol. Cells* **1998**, *54* (1-4), 39–48.
32. Raman, A. P.; Anoma, M. A.; Zhu, L.; Rephaeli, E.; Fan, S. Passive Radiative Cooling Below Ambient Air Temperature Under Direct Sunlight. *Nature* **2014**, *515*, 540–544.
33. Granqvist, C. G. Transparent Conductors as Solar Energy Materials: A Panoramic Review. *Sol. Energy Mater. Sol. Cells* **2007**, *91*, 1529–1598.
34. Yang, Y. -S.; Zhou, Y.; Chiang, F. B. Y.; Long, Y. Tungsten Doped VO2/Microgels Hybrid Thermochromic Material and Its Smart Window Application. *RSC Adv.* **2017**, 7, 7758–7762.
35. Rezaei, S. D.; Shannigrahi, S.; Ramakrishna, S. A Review of Conventional, Advanced, and Smart Glazing Technologies and Materials for Improving Indoor Environment. *Sol. Energy Mater. Sol. Cells* **2017**, *159*, 26–51.
36. Zhou, J.; Gao, Y.; Zhang, Z.; Luo, H.; Cao, C.; Chen, Z., et al. VO2 Thermochromic Smart Window for Energy Savings and Generation. *Sci. Rep.* **2013**, *3*, 3029.
37. Zhao, Y.; Xu, R.; Zhang, X.; Hu, X.; Knize, R. J.; Lu, Y. Simulation of Smart Windows in the ZnO/VO2/ZnS Sandwiched Structure with Improved Thermochromic Properties. *Energy Build* **2013**, *66*, 545–552.
38. Wu, C. -C.; Shih, W. -C. Development of a Highly Transparent, Low-Resistance Lithium-Doped Nickel Oxide Triple-Layer Film Deposited by Magnetron Sputtering. *Chem. Commun.* **2017**, *53*, 1634–1637.
39. Sharma, V.; Kumar, P.; Kumar, A.; Surbhi; Asokan, K.; Sachdev, K. High-Performance Radiation Stable ZnO/Ag/ZnO Multilayer Transparent Conductive Electrode. *Sol. Energy Mater. Sol. Cells* **2017**, *169*, 122–131.
40. Lin, T. -C.; Huang, W. -C.; Tsai, F. -C. Hydrogen Plasma Effect Toward the AZO/CuCr/AZO Transparent Conductive Electrode. *Microelectron Eng.* **2017**, *167*, 85–89.
41. Kim, D. -H.; Cho, K. -S.; Kim, H. -K. Thermally Evaporated Indium-Free, Transparent, Flexible SnO_2/AgPdCu/SnO_2 Electrodes for Flexible and Transparent Thin Film Heaters. *Sci. Rep.* **2017**, 7, 2550.
42. Chen, K. -N.; Yang, C. -F.; Wu, C. -C.; Chen, Y. -H. Development of the a-IGZO/Ag/a-IGZO Triple-Layer Structure Films for the Application of Transparent Electrode. *Materials* **2017**, *10*, 226.
43. Peres, L.; Bou, A.; Barakel, D.; Torchio, P. ZnS|Ag|TiO2 Multilayer Electrodes with Broadband Transparency for Thin Film Solar Cells. *RSC Adv.* **2016**, *6*, 61057–61063.
44. Meng-Qi, Z.; Han-Dong, J.; Peng-Qing, B.; Fu-Jian, Z.; Jin, M.; Xiao-Tao, H. Performance Improvement of TiO2/Ag/TiO2 Multilayer Transparent Conducting Electrode Films for Application on Photodetectors. *J Phys D Appl Phys* **2016,** *49*,115108. Dalapati, G.K. et al. *Prog Mater Sci* **2018**, *95*, 42-131, 115.
45. Kim, J. -H.; Kim, D. -H.; Kim, S. -K.; Bae, D.; Yoo, Y. -Z.; Seong, T. -Y. Control of Refractive Index by Annealing to Achieve High Figure of Merit for TiO2/Ag/TiO_2 Multilayer Films. *Ceram. Int.* **2016**, *42*, 14071–14076.
46. Kim, J. H.; Lee, H. -K.; Na, J. -Y.; Kim, S. -K.; Yoo, Y. -Z.; Seong, T. -Y. Dependence of Optical and Electrical Properties on Ag Thickness in TiO2/Ag/TiO_2 Multilayer Films for Photovoltaic Devices. *Ceram. Int.* **2015**, *41*, 8059–8063.

47. Kulczyk-Malecka, J.; Kelly, P. J.; West, G.; Clarke, G. C. B.; Ridealgh, J. A.; Almtoft, K. P., et al. Investigation of Silver Diffusion in TiO2/Ag/TiO2 Coatings. *Acta Mater.* **2014**, *66*, 396–404.
48. Alvarez, R.; González, J. C.; Espinós, J. P.; González-Elipe, A. R.; Cueva, A.; Villuendas, F. Growth of Silver on ZnO and SnO2 Thin Films Intended for Low Emissivity Applications. *Appl. Surf. Sci.* **2013**, *268*, 507–515.
49. Wu, H. -W.; Yang, R. -Y.; Hsiung, C. -M.; Chu, C. -H. Influence of Ag Thickness of Aluminum-Doped ZnO/Ag/Aluminum-Doped ZnO Thin Films. *Thin Solid Films* **2012**, *520*, 7147–7152.
50. Al-Kuhaili, M. F.; Al-Aswad, A. H.; Durrani, S. M. A.; Bakhtiari, I. A. Energy-Saving Transparent Heat Mirrors Based on Tungsten Oxide-Gold WO3/Au/WO3 Multilayer Structures. *Sol. Energy* **2012**, *86*, 3183–3189.
51. Neghabi, M.; Behjat, A.; Ghorashi, S. M. B.; Salehi, S. M. A. The Effect of Annealing on Structural, Electrical and Optical Properties of Nanostructured ZnS/Ag/ZnS Films. *Thin Solid Films* **2011**, *519*, 5662–5666.
52. Leng, J.; Yu, Z.; Xue, W.; Zhang, T.; Jiang, Y.; Zhang, J., et al. Influence of Ag Thickness on Structural, Optical, and Electrical Properties of ZnS/Ag/ZnS Multilayers Prepared by Ion Beam assIsted Deposition. *J. Appl. Phys.* **2010**, *108*, 073109.
53. Dobrikov, G. H.; Rassovska, M. M.; Andreev, N. M.; Boyadzhiev, S. I.; Gesheva, K. A.; Ivanova, T. M., et al. Development of Transparent Heat Mirrors Based on Metal Oxide Thin Film Structures. *Thin Solid Films* **2009**, *518*, 1091–1094.
54. Dalapati, G. K.; Masudy-Panah, S.; Chua, S. T.; Sharma, M.; Wong, T. I.; Tan, H. R., et al. Color Tunable Low Cost Transparent Heat Reflector Using Copper and Titanium Oxide for Energy Saving Application. *Sci. Rep.* **2016**, *6*, 20182.
55. Kim, H.; Kim, Y.; Kim, K. S.; Jeong, H. Y.; Jang, A. R.; Han, S. H., et al. Flexible Thermochromic Window Based on Hybridized VO_2/Graphene. *ACS Nano* **2013**, *7*, 5769–5776.
56. Liu, T.; Liu, B.; Wang, J.; Yang, L.; Ma, X.; Li, H., et al. Smart Window Coating Based on F-TiO2-KxWO3 Nanocomposites with Heat Shielding, Ultraviolet Isolating, Hydrophilic and Photocatalytic Performance. *Sci. Rep.* **2016**, *6*, 27373.
57. Lu, Q.; Liu, C.; Wang, N.; Magdassi, S.; Mandler, D.; Long, Y. Periodic Micro-Patterned VO_2 Thermochromic Films by Mesh Printing. *J. Mater. Chem. C* **2016**, *4*, 8385–8391.
58. Loka, C.; Park, K. R.; Lee, K. -S. Multi-Functional TiO2/Si/Ag(Cr)/TiNx Coatings for Low-Emissivity and Hydrophilic Applications. *Appl. Surf. Sci.* **2016**, *363*, 439–444.
59. Ko, E. -H.; Kim, H. -J.; Lee, S. -J.; Lee, J. -H.; Kim, H. -K. Nano-Sized Ag Inserted into ITO Films Prepared by Continuous Roll-to-Roll Sputtering for High-Performance, Flexible, Transparent Film Heaters. *RSC Adv.* **2016**, *6*, 46634–46642.
60. Kang, T. -W.; Kim, S. H.; Kim, C. H.; Lee, S. -M.; Kim, H. -K.; Park, J. S., et al. Flexible Polymer/Metal/Polymer and Polymer/Metal/Inorganic Trilayer Transparent Conducting Thin Film Heaters with Highly Hydrophobic Surface. *ACS Appl. Mater. Interfaces* **2017**, *9*, 33129–33136.
61. Zhao, Y.; Meek, G. A.; Levine, B. G.; Lunt, R. R. Near-Infrared Harvesting Transparent Luminescent Solar Concentrators. *Adv. Opt. Mater.* **2014**, *2*, 606–611.
62. Kamalisarvestani, M.; Saidur, R.; Mekhilef, S.; Javadi, F. S. Performance, Materials and Coating Technologies of Thermochromic Thin Films on Smart Windows. *Renew. Sustain. Energy Rev.* **2013**, *26*, 353–364.
63. Wang, Y.; Runnerstrom, E. L.; Milliron, D. J. Switchable Materials for Smart Windows. *Annu. Rev. Chem. Biomol. Eng.* **2016**, *7*, 283–304.
64. Béteille, F.; Livage, J. Optical Switching in VO_2 Thin Films. *J. Sol-Gel Sci. Technol.* **1998**, *13*, 915–921.
65. Karlsson, J.; Roos, A. Annual Energy Window Performance vs. Glazing Thermal Emittance-The Relevance of Very Low Emittance Values. *Thin Solid Films* **2001**, *392*, 345–348.

66. Ahmad, S. H. A.; Al-Kuhaili, M. F.; Durrani, S. M. A.; Faiz, M. M.; Ul-Hamid, A. Bi-Layered Energy Efficient Coatings as Transparent Heat Mirrors Based on Vanadium Oxide Thin Films. *Sol. Energy Mater. Sol. Cells* **2017**, *169*, 258–263.
67. Fan, J. C. C.; Bachner, F. J.; Foley, G. H.; Zavracky, P. M. Transparent Heat-Mirror Films of TiO_2/Ag/TiO_2 for Solar Energy Collection and Radiation Insulation. *Appl. Phys. Lett.* **1974**, *25*, 693–695.
68. Grosse, P.; Hertling, R.; Müggenburg, T. Design of Low Emissivity Systems Based on a Three-Layer Coating. *J. Non-Cryst. Solids* **1997**, *218*, 38–43.
69. Cheng, J.; Cao, G.; Zong, H.; Kang, C.; Jia, E.; Zhang, B., et al. Highly Transparent Conductive AZO/Zr50Cu50/AZO Films in Wide Range of Visible and Near Infrared Wavelength Grown by Pulsed Laser Deposition. *Results Phys.* **2017**, 7, 910–913.
70. Fang, Y.; He, J.; Zhang, K.; Xiao, C.; Zhang, B.; Shen, J., et al. Ar Plasma Irradiation Improved Optical and Electrical Properties of TiO_2/Ag/TiO_2 Multilayer Thin Film. *Opt. Lett.* **2015**, *40*, 5455–5458.
71. Chiu, P. -K.; Lee, C. -T.; Chiang, D.; Cho, W. -H.; Hsiao, C. -N.; Chen, Y. -Y., et al. Conductive and Transparent Multilayer Films for Low-Temperature TiO(2)/Ag/SiO(2) Electrodes by E-Beam Evaporation with IAD. *Nanoscale Res. Lett.* **2014**, *9*, 35.
72. Gong, L.; Lu, J.; Ye, Z. Conductive Ga Doped ZnO/Cu/Ga Doped ZnO Thin Films Prepared by Magnetron Sputtering at Room Temperature for Flexible Electronics. *Thin Solid Films* **2011**, *519*, 3870–3874.
73. Yang, X.; Gao, P.; Yang, Z.; Zhu, J.; Huang, F.; Ye, J. Optimizing Ultrathin Ag Films for High Performance Oxide-Metal-Oxide Flexible Transparent Electrodes Through Surface Energy Modulation and Template-Stripping Procedures. *Sci Rep* **2017**, 7, 44576. 116 Dalapati, G.K. et al. *Progr Mater Sci* **2018,** *95*, 42-131.
74. Dhar, A.; Alford, T. L. Optimization of TiO_2/Cu/TiO_2 Multilayer as Transparent Composite Electrode (TCE) Deposited on Flexible Substrate at room Temperature. *ECS Solid State Lett.* **2014**, *3*, N33–N36.
75. Leftheriotis, G.; Papaefthimiou, S.; Yianoulis, P. Integrated Low-Emittance-Electrochromic Devices Incorporating ZnS/Ag/ZnS Coatings as Transparent Conductors. *Sol. Energy Mater. Sol. Cells* **2000**, *61*, 107–112.
76. Cho, H.; Yun, C.; Park, J. -W.; Yoo, S. Highly Flexible Organic Light-Emitting Diodes Based on ZnS/Ag/WO3 Multilayer Transparent Electrodes. *Org. Electron.* **2009**, *10*, 1163–1169.
77. Leftheriotis, G.; Yianoulis, P.; Patrikios, D. Deposition and Optical Properties of Optimised ZnS/Ag/ZnS Thin Films for Energy Saving Applications. *Thin Solid Films* **1997**, *306*, 92–99.
78. Liu, X.; Cai, X.; Qiao, J.; Mao, J.; Jiang, N. The Design of ZnS/Ag/ZnS Transparent Conductive Multilayer Films. *Thin Solid Films* **2003**, *441*, 200–206.
79. Wu, C. -C.; Chen, P. S.; Peng, C. -H.; Wang, C. -C. TiO*x*/Ag/TiO*x* Multilayer for Application as a Transparent Conductive Electrode and Heat Mirror. *J. Mater. Sci. Mater. Electron* **2013**, *24*, 2461–2468.
80. Leftheriotis, G.; Yianoulis, P. Characterisation and Stability of Low-Emittance Multiple Coatings for Glazing Applications. *Sol. Energy Mater. Sol. Cells* **1999**, *58*, 185–197.
81. Ando, E.; Miyazaki, M. Durability of Doped Zinc Oxide/Silver/Doped Zinc Oxide Low Emissivity Coatings in Humid Environment. *Thin Solid Films* **2008**, *516*, 4574–4577.
82. Durrani, S. M. A.; Khawaja, E. E.; Al-Shukri, A. M.; Al-Kuhaili, M. F. Dielectric/Ag/Dielectric Coated Energy-Efficient Glass Windows for Warm Climates. *Energy Build* **2004**, *36*, 891–898.
83. Sivaramakrishnan, K.; Alford, T. L. Metallic Conductivity and the Role of Copper in ZnO/Cu/ZnO Thin Films for Flexible Electronics. *Appl. Phys. Lett.* **2009**, *94*, 052104.

84. Lampert, C. M. Coatings for Enhanced Photothermal Energy Collection I. Selective Absorbers. *Solar Energy Mater.* **1979**, *1*, 319–341.
85. Lampert, C. M. Heat Mirror Coatings for Energy Conserving Windows. *Solar Energy Mater.* **1981**, *6*, 1–41.
86. Ghasemi Varnamkhasti, M.; Fallah, H. R.; Mostajaboddavati, M.; Hassanzadeh, A. Influence of Ag Thickness on Electrical, Optical and Structural Properties of Nanocrystalline MoO_3/Ag/ITO Multilayer for Optoelectronic Applications. *Vacuum* **2012**, *86*, 1318–1322.
87. Ando, E.; Miyazaki, M. Moisture Resistance of the Low-Emissivity Coatings with a Layer Structure of Al-doped ZnO/Ag/Al-Doped ZnO. *Thin Solid Films* **2001**, *392*, 289–293.
88. Boiadjiev, S. I.; Dobrikov, G. H.; Rassovska, M. M. M. Preparation and Properties of RF Sputtered Indium-Tin Oxide Thin Films for Applications as Heat Mirrors in Photothermal Solar Energy Conversion. *Thin Solid Films* **2007**, *515*, 8465–8468.
89. Dhar, A.; Alford, T. L. High Quality Transparent TiO_2/Ag/TiO_2 Composite Electrode Films Deposited on Flexible Substrate at Room Temperature by Sputtering. *Appl. Mater.* **2013**, *1*, 012102.
90. Fan, J. C. C. Sputtered Films for Wavelength-Selective Applications. *Thin Solid Films* **1981**, *80*, 125–136.
91. Fang, X.; Mak, C. L.; Dai, J.; Li, K.; Ye, H.; Leung, C. W. ITO/Au/ITO Sandwich Structure for Near-Infrared Plasmonics. *ACS Appl. Mater. Interfaces* **2014**, *6*, 15743–15752.
92. Kim, H.; Kim, H. -S.; Ha, J.; Park, N. -G.; Yoo, S. Empowering Semi-Transparent Solar Cells with Thermal-Mirror Functionality. *Adv. Energy Mater.* **2016**, 6 1502466-n/a.
93. Kinoshita, T.; Nonomura, K. .; Jeon, N. J.; Giordano, F.; Abate, A.; Uchida, S.; Kubo, T.; Seok, S. L.; Nazeeruddin, M. K.; Hagfeldt, A.; Gratzel, M.; Segawa, H. Spectral Splitting Photovoltaics Using Perovskite and Wideband Dye-Sensitized Solar Cells. *Nat. Commun* **2015**, *6*, 8834.
94. Betancur, R.; Romero-Gomez, P.; Martinez-Otero, A.; Elias, X.; Maymo, M.; Martorell, J. Transparent Polymer Solar Cells Employing a Layered Light-Trapping Architecture. *Nat. Photon* **2013**, 7, 995–1000.
95. Zhou, E.; Nakano, M.; Izawa, S.; Cong, J.; Osaka, I.; Takimiya, K., et al. All-Polymer Solar Cell with High Near-Infrared Response Based on a Naphthodithiophene Diimide (NDTI) Copolymer. *ACS Macro Lett* **2014**, *3*, 872–875.
96. Za Tan; Li, S.; Wang, F.; Qian, D.; Lin, J.; Hou, J., et al. High Performance Polymer Solar Cells with As-Prepared Zirconium Acetylacetonate Film as Cathode Buffer Layer. *Sci. Rep.* **2014**, *4*, 4691.
97. Xia, X.; Wang, S.; Jia, Y.; Bian, Z.; Wu, D.; Zhang, L., et al. Infrared-Transparent Polymer Solar Cells. *J. Mater. Chem.* **2010**, *20*, 8478–8482.
98. Chen, C. -C.; Dou, L.; Zhu, R.; Chung, C. -H.; Song, T. -B.; Zheng, Y. B., et al. Visibly Transparent Polymer Solar Cells Produced by Solution Processing. *ACS Nano* **2012**, *6*, 7185–7190.
99. Huang, X.; Han, S.; Huang, W.; Liu, X. Enhancing Solar Cell Efficiency: The Search for Luminescent Materials as Spectral Converters. *Chem. Soc. Rev.* **2013**, *42*, 173–201.

Further readings

1. Cao, F.; Kenneth, M.; Gang, C.; Zhifeng, R. A Review of Cermet-Based Spectrally Selective Solar Absorbers. *Energy Environ. Sci.* **2014**, 7 (5), 1615.
2. McGuire, J. A.; Joo, J.; Pietryga, J. M.; Schaller, R. D.; Klimov, V. I. New Aspects of Carrier Multiplication in Semiconductor Nanocrystals. *Acc. Chem. Res.* **2008**, *41* (12), 1810–1819.